Nearly bound states in the radiation continuum in a circular array of dielectric rods

Evgeny N. Bulgakov[1,2] and Almas F. Sadreev[1]

[1]*Kirensky Institute of Physics, Federal Research Center KSC SB RAS, 660036 Krasnoyarsk, Russia*
[2]*Siberian State University of Science and Technology, Krasnoyarsk 660037, Russia*

We consider E-polarized bound states in the radiation continuum (BICs) in circular periodical arrays of N infinitely long dielectric rods. We find that each true BIC which occurs in an infinite linear array has its counterpart in the circular array as a near-BIC with extremely large quality factor. We argue analytically as well as numerically that the quality factor of the symmetry-protected near-BICs diverges as $e^{\lambda N}$, where λ is a material parameter dependent on the radius and the refraction index of the rods. By tuning of the radius of rods, we also find numerically non-symmetry-protected near-BICs. These near-BICs are localized with exponential accuracy outside the circular array, but fill the whole inner space of the array carrying orbital angular momentum.

I. INTRODUCTION

Recently confined electromagnetic modes above the light line, bound states in the continuum (BICs) were shown to exist in periodic arrays of long dielectric rods [1–18]. Among the numerous types of BICs, it is worthwhile to emphasize the BICs which can propagate either cross to rods [10,17] or along the axis of periodicity of the system [7]. In practice, there are no infinite arrays of rods. In the array of a finite number of rods, the BICs become quasi-BICs with finite Q factor which diverges as N^2 for the symmetry-protected BICs or even as N^3 for the non-symmetry-protected BICs with tuned radius of rods [19,20]. These results are in agreement with the theorem on the absence of BICs in the bounded domain which is a complement of an unbounded domain [21,22]. The BICs can appear only in an unbounded domain. The physical occurrence of the BICs in the infinite array of rods is a result of periodicity of the array that quantizes the radiation continua in the form of diffraction continua [10,23]. Then, if the frequency is below the cutoff of the second diffraction continuum, the BIC is embedded into the first diffraction continuum. Note that the second diffraction continuum is also important, providing a bound space for the BIC [10].

Moreover, the scattering of acoustic waves and water surface waves by an array of cylinders was extensively studied in a series of papers [24,25]. The remarkable case of a circular array of cylinders was considered in Refs. [26–29]. Numerical results of strong confinement of light in a circular array of dielectric pillars [30] and symmetry-protected quasi-BICs with exponentially high quality factor in the circular array of dielectric nanorods [31] were reported recently. We reexamine these results for E-polarized symmetry-protected BICs in the circular array of N infinitely long cylindrical dielectric rods and demonstrate the patterns of quasi-BICs with extremely large quality factors. Following [28], we define such BICs as near-BICs.

We present mathematical arguments in favor of exponentially large quality factors of the symmetry-protected near-BICs in the circular array of dielectric rods. In addition, we

find numerically the non-symmetry-protected near-BICs by tuning the rod radius. In contrast to the symmetry-protected near-BICs, they fill the internal space of the circular array. The circular array of rods supports non-symmetry-protected near-BICs with orbital angular momentum (OAM). Finally, we demonstrate the counterparts of the BICs in the linear array embedded into two and three diffraction continua which fill only a part of the inner space of the circular array. The diffraction continua for the linear chain are given by plane waves,

$$E_z(x,y) = e^{iq_{y,p}y + i(q_p+q_x)x}, \tag{1}$$

where

$$q_{y,p} = \sqrt{k_0^2 - (q_x + q_p)^2}, \quad q_p = \frac{2\pi p}{h}, \tag{2}$$

and $p = 0, \pm 1, \pm 2, \ldots$ enumerates the diffraction continua for the periodical chain of rods with the period h.

II. SCATTERING THEORY FOR CIRCULAR ARRAY OF CYLINDERS

Following Ref. [32] (see quite similar procedure described in Ref. [24] for the Neumann boundary conditions at the surfaces of rigid cylinders), we present the general E-polarized solution at the vicinity of the jth rod for the electric field directed along the rods as follows:

$$E_z(r_j,\phi_j) = E_{\text{inc}} + \sum_m \big[a_m(j)J_m(k_0 r_j)$$
$$+ b_m(j)H_m^{(1)}(k_0 r_j)\big]e^{im\phi_j}, \tag{3}$$

where the first term presents the incident wave from a pointlike source placed at the center of circular array $x = 0, y = 0$, as sketched in Figs. 2 and 3,

$$E_{\text{inc}} = H_n^{(1)}(k_0 r)e^{in\phi}; \tag{4}$$

the second term is a contribution of the other rods and the field emanating from the jth rod. ϕ_j and r_j are the polar coordinates of the radius vector $\mathbf{r}_j$ in the local coordinate systems of the
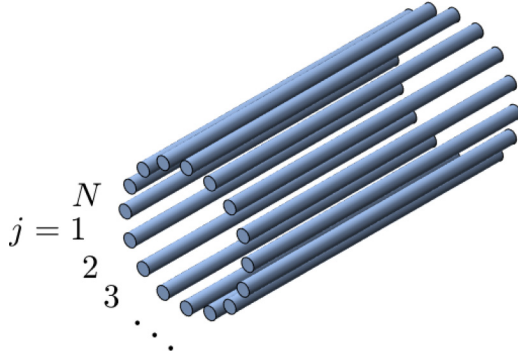
FIG. 1. N infinitely long circular dielectric rods with radius a are stacked parallel to each other on the surface of a cylinder with the radius R, which is measured in terms of the distance between the centers of the nearest rods.

jth rod, as shown in Figs. 1 and 2. We introduce substitutions,

$$a_m(j) = \widetilde{a}_m(j)e^{-im\alpha_j}, \quad b_m(j) = \widetilde{b}_m(j)e^{-im\alpha_j}, \quad (5)$$

where $\alpha_j = \frac{2\pi(j-1)}{N}$ (see Fig. 2), and we use the Graf formula [32],

$$H_m^{(1)}(k_0 r_j(P))e^{im\phi_j}$$
$$= \sum_{m'} e^{i(m-m')\theta_{jl}} H_{m'-m}^{(1)}(k_0 r_{jl}) J_{m'}(k_0 r_l(P))e^{i\phi_l(P)}, \quad (6)$$

where definitions of angles and distances are shown in Fig. 2. That allows us to write the following relations between the amplitudes $\widetilde{a}_m$ and $\widetilde{b}_m$:

$$\widetilde{a}_m(j) = \sum_{l \neq j}^{N} \sum_{m'} \widetilde{b}_{m'}(l) \exp[im\alpha_j - im'\alpha_l - i(m-m')\theta_{lj}]$$
$$\times H_{m-m'}^{(1)}(k_0 r_{lj}). \quad (7)$$
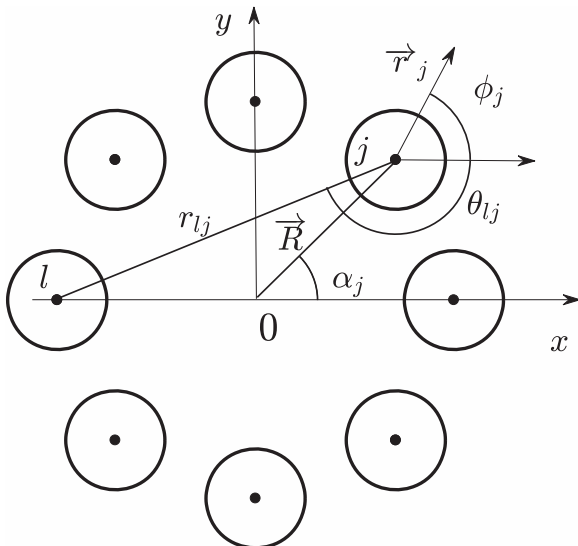

FIG. 2. Plan view of circular periodical array of rods.

Periodicity of the circular array of rods allows us to write

$$\widetilde{a}_{mn}(j) = \widetilde{a}_{mn}(1)e^{ik_n(j-1)},$$
$$\widetilde{b}_{mn}(j) = \widetilde{b}_{mn}(1)e^{ik_n(j-1)}, \quad k_n = 2\pi n/N,$$
$$n = 0, 1, 2, \dots, N-1, \quad (8)$$

where k_n is the Bloch number. In particular, for $j = 1$, we have, from Eqs. (7) and (8),

$$\widetilde{a}_{mn}(1) = \sum_{l=2}^{N} \sum_{m'} \widetilde{b}_{m'n}(1) \exp[ik_n(l-1)$$
$$- i(m-m')\theta_{l1} - im'\alpha_l] H_{m-m'}^{(1)}(k_0 r_{lj}). \quad (9)$$

Finally, we close Eq. (9), which relates incident amplitude $\widetilde{a}_{mn}(1)$ with emanating amplitude $\widetilde{b}_{mn}(1)$, by the following equation:

$$\widetilde{b}_{mn}(1) = S_m[\widetilde{a}_{mn}(1) + \psi_{\text{inc},m}^n], \quad (10)$$

where S_m is the diagonal component of the S matrix of a circular dielectric rod,

$$S_m = \frac{\sqrt{\epsilon} J_m'(qa) J_m(k_0 a) - J_m'(k_0 a) J_m(qa)}{H_m^{(1)'}(k_0 a) J_m(qa) - \sqrt{\epsilon} J_m'(qa) H_m^{(1)}(k_0 a)}, \quad (11)$$

$q = \sqrt{\epsilon} k_0$, and ϵ is the permittivity of the rod of radius a. Substituting Eq. (10) into Eq. (9), we can formulate the basic equation

$$\sum_{m'} L_{mm'}^n \widetilde{b}_{m',n}(1) = \psi_{\text{inc},m}^n, \quad (12)$$

where the matrix elements are given by

$$L_{mm'}^n = -S_m \sum_{l=2}^{N} \exp[ik_n(l-1) + i(m'-m)\theta_{l1} - im'\alpha_l]$$
$$\times H_{m-m'}^{(1)}(k_0 r_{l1}) + \delta_{mm'}, \quad (13)$$

and, according to Eq. (4),

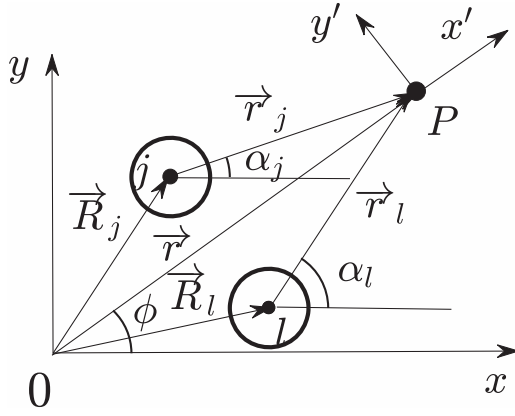$$\psi_{\text{inc},m}^n = S_m H_{n-m}^{(1)}(k_0 R). \quad (14)$$

III. FAR-FIELD ZONE SOLUTION

Outside the rods for $r_j > a$, the solution with the Bloch wave number k_n takes the following form [32]:

$$E_{z,n} = \sum_m \sum_{j=1}^{N} \widetilde{b}_{mn}(1) \exp[ik_n(j-1) + im(\phi_j - \alpha_j)]$$
$$\times H_m^{(1)}(k_0 r_j)e^{im\phi_j}. \quad (15)$$

Now we can write the electric field in the far-field zone $r_j \gg R$ at the point P shown in Fig. 3 by the use of the asymptotic form of the Hankel function,

$$H_m^{(1)}(x) \approx \sqrt{\frac{2}{\pi x}} \exp[-i\pi(2m+1)/4 + ix]. \quad (16)$$

FIG. 3. The point P in the far-field zone.

We have $\overrightarrow{r} = \overrightarrow{R}_j + \overrightarrow{r}_j$, where all three radius vectors are shown in Fig. 3. For $r \gg R$, we can approximate

$$\sqrt{\frac{1}{k_0 r_j}} \exp(i k_0 r_j) \approx \sqrt{\frac{1}{k_0 r}} \exp[i k_0 r - i k_0 R \cos(\alpha_j - \phi)]. \tag{17}$$

Therefore, in the far-field zone, the electric field can be approximated as follows:

$$E_{z,n} \approx \sqrt{\frac{2}{k_0 r}} e^{i k_0 r - i\pi/4} \sum_m (-i)^m \widetilde{b}_{mn} \sum_{j=1}^{N} \exp[i k_n (j-1)$$
$$+ i m(\phi - \alpha_j) - i k_0 R \cos(\alpha_j - \phi)]. \tag{18}$$

Now we apply to this equation a mathematical observation of the exponential convergence of the sums [33],

$$I_N = \frac{1}{N} \sum_{k=1}^{N} u(e^{2\pi i k/N}). \tag{19}$$

The sum is converged as follows:

$$|I_N - I| \leqslant \frac{\max(u)}{s^N - 1}, \tag{20}$$

for some $s > 1$, and

$$I = \frac{1}{2\pi} \int_0^{2\pi} d\theta u(e^{i\theta}), \tag{21}$$

where $u(\theta) = u(\theta + 2\pi)$ is a periodical analytical function. Therefore, we can write Eq. (18) as follows:

$$E_{z,n} = N e^{in\phi} \sum_m (-i)^m \widetilde{b}_{mn} \sqrt{\frac{2}{k_0 r}} e^{i k_0 r - i\pi/4} \frac{1}{2\pi}$$
$$\times \int_0^{2\pi} d\tau \exp[-i\tau(m-n) - i k_0 R \cos\tau]$$
$$+ O(e^{-\lambda N}). \tag{22}$$

Using the identity for the Bessel functions,

$$J_n(z) = \frac{i^{-n}}{\pi} \int_0^{\pi} e^{iz\cos\tau} \cos(n\tau) d\tau, \tag{23}$$

we have, for the electric field (22) in the far zone,

$$E_z = E_{\text{inc}} + N e^{in\phi} \sqrt{\frac{2}{k_0 r}} e^{i k_0 r - i\pi/4} (-i)^n$$
$$\times \sum_m \widetilde{b}_{mn} J_{n-m}(k_0 R) + O(e^{-\lambda N}). \tag{24}$$

IV. THE SOLUTION INSIDE THE CIRCULAR ARRAY OF RODS

Now we consider the solution inside the circular array. We have, for the electric field,

$$E_{z,n} = \sum_m \widetilde{b}_{mn} \sum_{j=1}^{N} e^{i(n-m)\alpha_j} H_m^{(1)}(k_0 r_j) e^{im\phi_j}. \tag{25}$$

Let us use the Graf formula in order to transfer the solution at a local position defined by $\overrightarrow{r}_j = (r_j, \phi_j)$ to the solution in the global system of coordinates defined by the radius vector $\overrightarrow{r} = (r, \phi)$. We have

$$H_m^{(1)}(k_0 r_j) e^{im\phi_j} = \sum_{m'} e^{i(m-m')\alpha_j} H_{m'-m}^{(1)}(k_0 R) J_{m'}(k_0 r) e^{im'\phi}. \tag{26}$$

Substitution of this equation into Eq. (25) gives

$$E_{z,n} = \sum_m \widetilde{b}_{mn} \sum_{m'} \sum_{j=1}^{N} e^{i(k_n - k_{m'})(j-1)} H_{m'-m}^{(1)}(k_0 R) J_{m'}(k_0 r) e^{im'\phi}. \tag{27}$$

Due to the equality

$$\sum_{j=1}^{N} e^{i2\pi(j-1)(m-m')/N} = N\delta(m - m' - qN), \tag{28}$$

where q is an integer, we can simplify Eq. (27) as follows:

$$E_{z,n} = N \sum_{m,q} \widetilde{b}_{mn} H_{n+qN-m}^{(1)}(k_0 R) J_{n+qN}(k_0 r) e^{i(n+qN)\phi}. \tag{29}$$

V. NEAR-BICs

For the infinite periodic arrays, if a source is switched off, there are exceptional cases with selected real eigenfrequencies embedded into the radiation continuum, as was briefly reviewed in Sec. I. These exceptional cases define BICs which are localized in the vicinity of the arrays [1–18]. Let us consider what happens to these BICs if one were to roll up a finite array into a circle. For the solution to vanish in the far-field zone, we have to imply that all $\widetilde{b}_{mn} = 0$ [22]. That, in turn, requires that there is also no electric field in the near zone, according to Eq. (25), i.e., the solution equals zero everywhere. However, if only exponential smallness is required in the far-field zone, for $N \gg 1$, we can imply a softer condition for the amplitudes,

$$\sum_m \widetilde{b}_{mn} J_{n-m}(k_0 R) = 0, \tag{30}$$

as seen from Eq. (24). Therefore, the solution turns to zero in the far-field zone with exponential accuracy, while in the

near-field zone, the solution given by Eq. (29) is finite and is referred to as a near-BIC.

Now we show that this formulation of the near-BICs in the circular arrays is consistent with source-free Eq. (12),

$$\widehat{L}\Psi_c = 0, \tag{31}$$

which has no solution for real frequencies. However, by analytical continuation of the frequency k_0 into the complex plane $\mathrm{Re}(k_0) + i\mathrm{Im}(k_0)$, we can find a solution of Eq. (31) which has an extremely small imaginary part, $-\mathrm{Im}(k_0) \sim e^{-\lambda N}$. Numerics show that the corresponding eigenmode Ψ_c satisfies Eq. (30).

A. The symmetry-protected near-BICs

We start with a consideration of the solution which is odd relative to $y' \rightarrow -y'$ in the local system of coordinates, as sketched in Fig. 3. For $k_n = 0$ (standing waves), we can take all amplitudes $\widetilde{a}_m(j)$ and $\widetilde{b}_m(j)$ independent of the site index j. Hence, we can rewrite the solution (3) in the vicinity of the rods as follows:

$$E_{z,\text{even}} = \sum_{m=0}^{\infty} \left[\widetilde{a}_{2m+1}J_{2m+1}(k_0 r_j) + \widetilde{b}_{2m+1}(j)H_{2m+1}^{(1)}(k_0 r_j) \right]$$
$$\times \sin[(2m+1)(\phi_j - \alpha_j)], \tag{32}$$

$$E_{z,\text{odd}} = \sum_{m=1}^{\infty} \left[\widetilde{a}_{2m}(j)J_{2m}(k_0 r_j) + \widetilde{b}_{2m}(j)H_{2m}^{(1)}(k_0 r_j) \right]$$
$$\times \sin[2m(\phi_j - \alpha_j)]. \tag{33}$$

For the odd solution, we imply the following equalities:

$$\widetilde{b}_{2m+1} = \widetilde{b}_{-2m-1},$$
$$\widetilde{b}_{2m} = -\widetilde{b}_{-2m}. \tag{34}$$

Then Eq. (30) is fulfilled. For the directional array of an infinite number of rods, the most trivial symmetry-protected BIC is the solution which is odd relative to each rod in the array direction. The solution of the symmetry-protected BIC is presented in Refs. [10,11]. Then the coupling of the BIC with the first diffraction continuum obviously equals zero.

Below we hold in numerics two parameters of dielectric rods fixed: the permittivity $\epsilon = 15$ (silicon rods) and the period $h = 2\pi R/N$ (the angular distance between the centers of the rods). In what follows, all other lengths are measured in terms of this period. The frequency k_0 is measured in terms of c/h, where c is the light velocity. In Fig. 4, we show how the pole of the matrix $\widehat{L}$ behaves with the growth of the number of rods for different types of the symmetry-protected near-BICs. One can see that the real part of this complex eigenvalue limits the frequency of the symmetry-protected true BIC in the infinite array of rods. Figure 5(a) shows the pattern of electric field E_z of the symmetry-protected BIC in the linear array of dielectric rods. Figures 5(b) and 5(c) show its circular counterparts in the circular array of 15 and 25 rods, respectively. Figure 6 shows other examples of the symmetry-protected near-BICs.

The patterns of the near-BICs, as well as their exponentially large Q factors, point out an analogy with the whispering-gallery modes (WGMs), as shown in Fig. 5(d), which also show
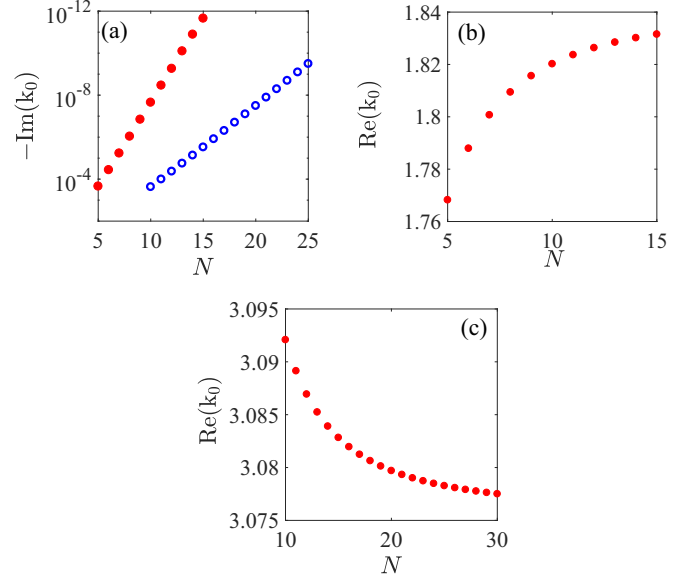

FIG. 4. The pole of the inverse of matrix (13) exponentially small in the imaginary part vs the number of rods for the symmetry-protected near-BIC shown in Figs. 5 and 6 with the parameters $\epsilon = 15$, $a = 0.44$. (a) Imaginary part and (b),(c) real part of the pole.

an exponentially large Q factor [34]. However, in the present case, the Q factor is proportional to $Q \sim \exp(\lambda N)$, while for the WGM, $Q \sim \exp(\kappa m)$, where m is the order of the Bessel function. Finally, in Fig. 7, we present numerical results for the parameter λ as dependent on the material parameters.
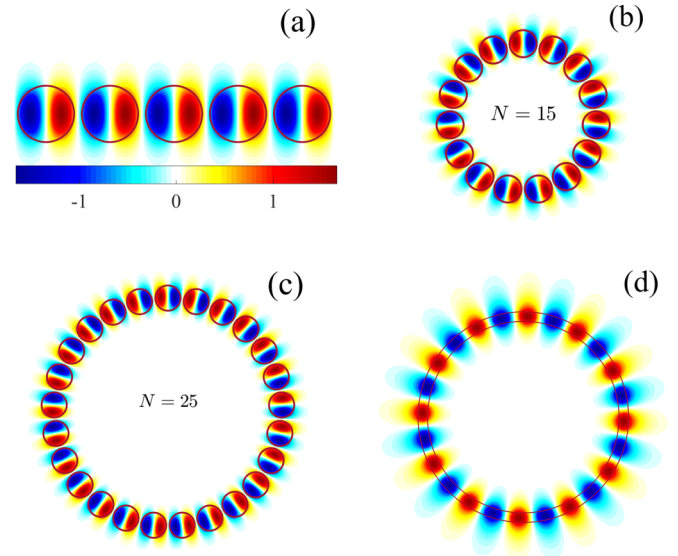

FIG. 5. Profiles of the electric field directed along the rods. (a) Fragment of the profile of the true symmetry-protected BIC in a linear array with the frequency $k_0 = 1.8412$ and (b),(c) its counterparts in a circular array of 15 rods with the frequency $k_0 = 1.8315$ and the Q factor $Q = 2 \times 10^{11}$, and 25 rods with the frequency $k_0 = 1.837$ and the Q factor $Q = 2 \times 10^{20}$, respectively, for $\epsilon = 15, a = 0.44$. (d) Whispering-gallery mode with angular momentum $m = 12$ and frequency $k_0 = 0.45304, Q = 1.1 \times 10^7$ in a circular tube shown by solid lines.
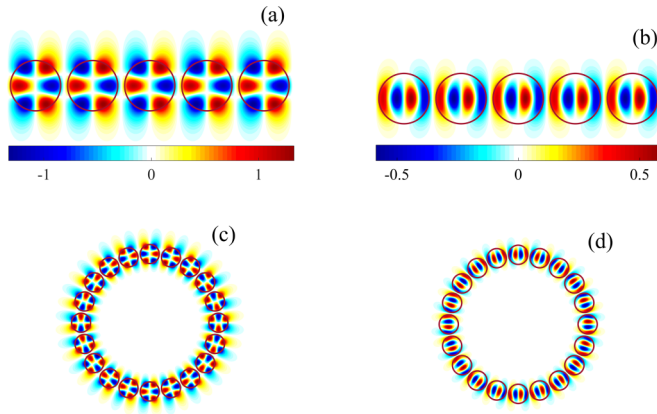
FIG. 6. Patterns of the symmetry-protected BICs with $k_n = 0$ in (a),(b) a linear infinite array of rods and (c),(d) their counterparts in a circular array of 20 rods. The parameters of the BICs are the following: (a) $a = 0.44, k_0 = 3.0758$, (b) $a = 0.44, k_0 = 3.5553$, (c) $a = 0.44, k_0 = 3.0797, Q = 4.8 \times 10^7$, (d) $k_0 = 3.5461$, $Q = 1.2 \times 10^7$.

B. Non-symmetry-protected near-BICs embedded into the first diffraction continuum

However, the above analogy of near-BICs in the circular array of rods with the WGMs is terminated to consider the non-symmetry-protected near-BICs which need tuning of the rod radius. One of the examples of true BICs, borrowed from Refs. [10,17], is shown in Fig. 8(a). Its counterpart in the circular array is even for $k_n = 0$ relative to $y' \rightarrow -y'$ in the local system of coordinates. In that case, Eq. (30) can be fulfilled by tuning, for example, the rod radius a. Figures 8(b)–8(d) demonstrate what happens with this BIC if one were to roll up the rods in a circle and then optimize the rod radius a. Because of the symmetry of the infinite array of rods with respect to up and down by tuning of the rod radius, we can achieve zero coupling of the BIC with both half radiation spaces above and below the array. In the circular array of rods, we can achieve extremely small coupling of the near-BIC to trap light against emanation outside the circle. However, we cannot simultaneously suppress emanation inside the circle. As a result, one can see that the near-BIC fills the whole inner space of the circular array, as demonstrated in Figs. 8(b)–8(d).

The next aspect of the non-symmetry-protected near-BICs is related to dependence of the Q factor on N. For each N, the near-BIC needs optimization of the rod radius to give rise to

FIG. 8. (a) Fragment of the electric-field profile of the non-symmetry-protected BIC in a linear array with the radius $a = 0.44441$ and the frequency $k_0 = 2.8299$. Its counterparts with $k_n = 0$ in the circular array are (b) 20 rods with $a = 0.43087, k_0 = 2.9234$, $Q = 1.5 \times 10^8$, (c) 10 rods with $a = 0.43087, k_0 = 2.9258, Q = 150$, and (d) 27 rods with $a = 0.43087, k_0 = 2.9251, Q = 5000$.

an extremely large Q factor, similar to the symmetry-protected near-BICs [see Fig. 4(a)]. However, in practice, it is easier to optimize the rod radius for some selected number of rods. Currently, we have selected $N = 20$. Then, a change of the number of rods with the same radius a gives the dependence of the Q factor, shown in Fig. 9, which has nonmonotonic behavior. One can see that for all N except $N = 20$, the circular array of rods can support only resonances with the Q factors in the range from hundreds to tens of thousands.

Let us leave the material parameters unchanged, but take the number of rods, say, $N \neq 20$. Then the solution becomes a resonant state which strongly emanates the electromagnetic (EM) field into the first diffraction radiation continuum, as
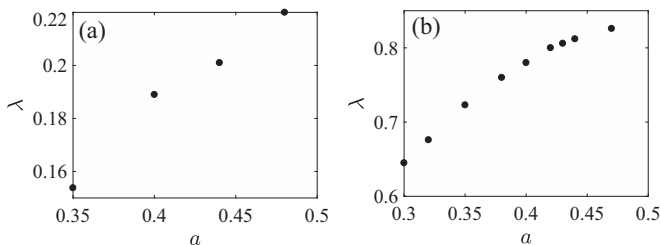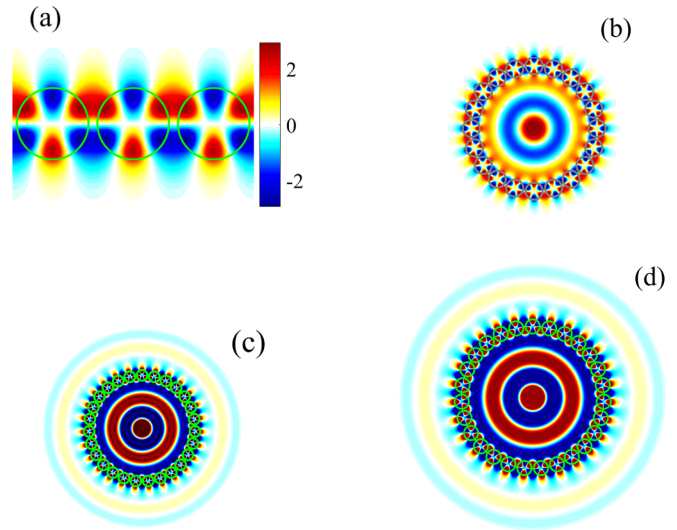

FIG. 7. Dependence of the parameter λ which defines the Q factor $e^{\lambda N}$ vs the radius of rods for the symmetry-protected near-BICs at (a) $\epsilon = 3$ and (b) $\epsilon = 15$.
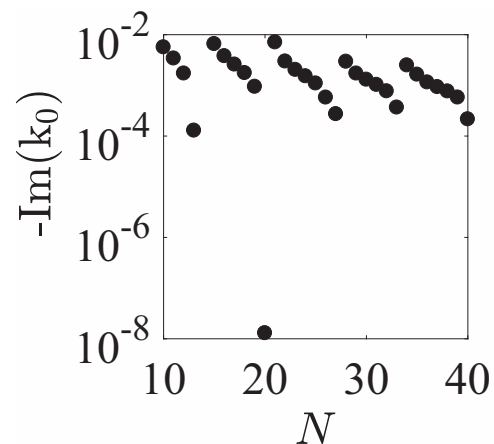

FIG. 9. The imaginary part of the frequency in logarithmic scale vs the number of rods for the case of the non-symmetry-protected BIC shown in Fig. 8(b) with the rod radius $a = 0.4387$ optimized for the case $N = 20$.
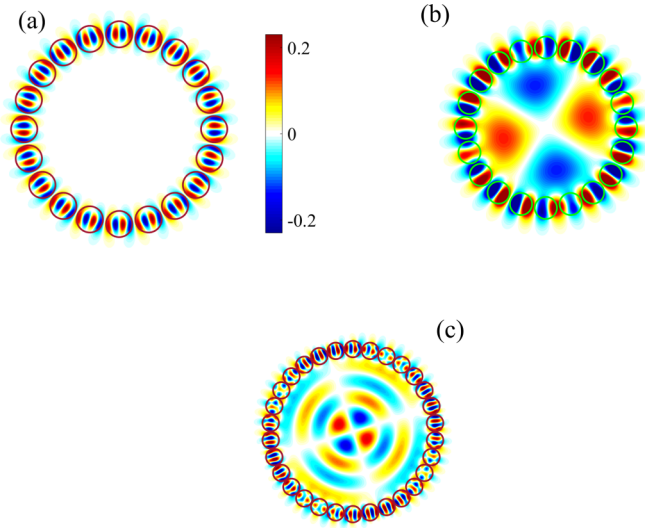
FIG. 10. Patterns of the non-symmetry-protected Bloch BIC in a circular array of rods $N = 20$. (a) $n = 1, a = 0.46636, k_0 = 1.7722$, $Q = 1.3 \times 10^7$, (b) $n = 2, a = 0.4389, k_0 = 1.7663, Q = 2.5 \times 10^6$, and (c) $N = 30, a = 0.47745, k_0 = 3.39887, n = 2, Q = 5.3 \times 10^8$.

shown in Figs. 8(c) and 8(d). The quality factors are taken from Fig. 9.

Until now, we considered near-BICs with the zero Bloch vector $k_n = 0$, i.e., with no angular dependence, as seen from Fig. 8(b). Figure 10 shows the near-BIC with OAM $n = 1$ and $n = 2$ with high Q factor. However, if one wants to consider the near-BIC with lower Q factor, one can see distinctively as such a near-BIC decays into the radiation continuum. Figure 11(a) shows the pattern of true non-symmetry-protected BIC in the linear array. If one does not tune the radius of the rods after rolling up into a circular array, the BIC transforms into the near-BIC with moderate Q factor around 10^3, as seen from Fig. 9. As a result, one can distinctively see in Fig. 11(b) as such a near-BIC emanates into the radiation continuum following its OAM which equals 4.

C. BICs embedded into a few diffraction continua

In the infinite linear array of rods, there are BICs embedded into a few diffraction continua given by Eqs. (1) and (2). They are symmetry protected relative to the first continuum and are tuned by the radius of rods to be embedded into the

FIG. 12. (a) Pattern of the non-symmetry-protected BIC embedded into two diffraction continua in a linear infinite array of rods and (b) their counterparts in the circular array of 40 rods. The parameters of BICs are the following: (a) $a = 0.24326, k_0 = 7.2946$, (b) $a = 0.2626, k_0 = 6.8092, Q = 8.5 \times 10^8$.

higher continua. [10]. Owing to high frequencies, these BICs occur at the rod radius that is smaller compared to the BICs embedded into the first diffraction continuum only. In this section, we present their circular counterparts. We begin with the BIC embedded into the first and second diffraction continua given by $p = 0$ and $p = 1$ of the linear array of rods for $\pi < k_0 < 3\pi$. It has the Bloch vector along the circular array equal to $\beta = \pm \pi / h$ [10], as shown in Fig. 12(a). Respectively, its circular counterpart has the same Bloch vector, $k_{N/2} = \pm \pi$.

Figure 13(a) presents the BIC with the Bloch vector $\beta = 0$ embedded into three diffraction continua with $p = 0, p = \pm 1$ for $2\pi < k_0 < 4\pi$ [10], and Fig. 13(b) shows its circular counterpart. However, in order to achieve high Q factors of these BICs, the number of rods is to be rather high, i.e., 40 and 50.

Above we have presented the symmetry-protected BICs which localize around the rods (see Figs. 5 and 6) and non-symmetry-protected BICs which fill the whole inner space of the circular array (see Figs. 8, 10, and 11). One can see that BICs embedded into two or more diffraction continua (see Figs. 12 and 13) have a radial range of localization that is less than the radius of circle R. That radial behavior of the BICs is the result of radial behavior of the Bessel functions of a high order. For $\nu \ll 1$, we have an asymptote through the Airy function [35],

$$J_\nu(\nu + z\nu^{1/3}) \sim 2^{1/3}\nu^{-1/3}\mathrm{Ai}(-2^{1/3}z) + O(\nu^{-1}).$$
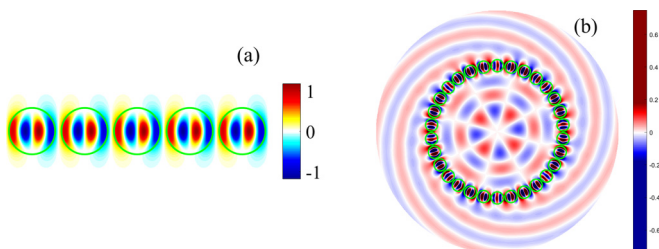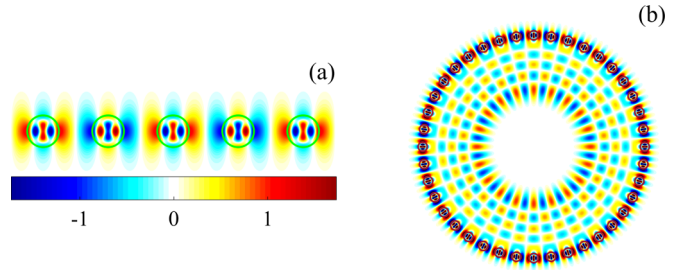

FIG. 11. (a) Pattern of the BIC in the linear array with the parameters $a = 0.44, k_0 = 3.5553$ and (b) its circular counterpart, the near-BIC with the parameters $a = 0.44, k_0 = 3.4469, n = 4, Q = 2.6 \times 10^3$.
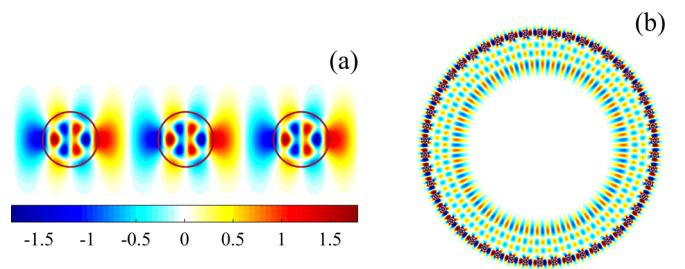

FIG. 13. (a) Pattern of the non-symmetry-protected BIC embedded into three diffraction continua in a linear infinite array of rods and (b) their counterparts in the circular array of 50 rods. The parameters of BICs are the following: (a) $a = 0.2386, k_0 = 8.9518$, (b) $a = 0.2335, k_0 = 9.1298, Q = 1.1 \times 10^{14}$.
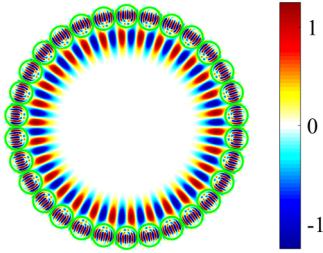
FIG. 14. Pattern of the near-BIC embedded into three diffraction continua in the circular array of 30 rods with the following parameters: $a = 0.48365, k_0 = 8.3214, Q = 1.852 \times 10^{11}$.

The Airy function tends to zero when its argument exceeds zero. From Eq. (29), we have $\nu = n + qN$ and $z = k_0 r$. Therefore, the radial width of BIC localization can be evaluated as

$$\Delta = R - r \sim R - \frac{n + qN}{k_0}. \tag{35}$$

If the BIC is embedded into only the first diffraction continuum, we have $k_0 < 2\pi$. Then, from Eq. (35), we obtain that the near-BIC occupies the whole inner region inside the circle. For the near-BIC embedded into the first and second diffraction continua, we have $\pi < k_0 < 3\pi$ that gives

$$\Delta \sim R - \frac{N}{2k_0} = N\left(\frac{1}{2\pi} - \frac{1}{2k_0}\right).$$

In particular, for the near-BIC shown in Fig. 13, we have $n = N/2, q = 0$ and $k_0 = 6.8$ to obtain $\Delta \sim R(1 - \pi/k_0) = 0.54R$ that is close the numerical result shown in Fig. 13. At last, for the BIC embedded into three continua, we have $n = 0, k_0 = 8.32$ and, respectively, from Eq. (35) we obtain

$$\Delta \sim R\left(\frac{1}{2\pi} - \frac{1}{k_0}\right) \approx \frac{R}{4},$$

which again is in good agreement with Fig. 14. Surprisingly, we revealed the near-BIC with $Q = 1.85 \times 10^{11}$ shown in Fig. 14 in the circular array of 30 rods whose linear counterpart is not the BIC, but the narrow resonance.

VI. SUMMARY

We considered light trapping by a circular array of infinitely long dielectric rods. Each BIC, both symmetry protected and non-symmetry protected, existing in the linear arrow of rods [10,11,17] has its circular counterpart, i.e., near-BICs.

Although the trapped light modes cannot be rigorously considered as the BIC in the circular array of rods because of arguments presented in Refs. [21,22], we have presented analytical arguments in favor that the Q factor of the symmetry-protected near-BICs with zero Bloch number grows exponentially with the number of rods. This numerically important result is presented in Fig. 4(a) and independently by Lu and Liu [31]. In particular, for 25 rods, the Q factor of the symmetry-protected trapped modes reaches values of the order of 10^{15}, similar to the whispering-gallery modes, as demonstrated in Fig. 5. In practice, such Q factors make the near-BICs in the circular array indistinguishable from the true BIC in the infinite array of rods that allowed us to define them as the near-BICs. The symmetry-protected near-BICs with zero Bloch number are close in nature to the whispering-gallery modes (WGMs) [see Fig. 5(d)], whose high Q factor is explained by total internal reflection and not by destructive interference.

However, the analogy with the WGM is ended if one is to proceed to the symmetry-protected near-BICs with nonzero Bloch number or the non-symmetry-protected near-BICs. The cardinal difference between these near-BICs and the WGM is that the former fills the whole inner space of the circular array. As dependent on the Bloch vector $k_n = 2\pi n/N, n = 0, 1, 2, \ldots$, the inner structure of the near-BIC defines the orbital angular momentum (OAM) with respect to the circular array and irrespectively of the solution inside the individual rod. After an abrupt change of the radius of the circle, these near-BICs with OAM emanate in the surrounding space in the form shown in Fig. 11. Also, the Q factor of the non-symmetry-protected near-BICs that is reached can be extremely large; however, we cannot conclude that there is exponential behavior of the Q factor with the number of rods N because of the necessity to tune the radius of the rods for each N. As it was shown in Ref. [10], there are BICs in the infinite linear array of rods embedded into a few diffraction continua. In the present paper, we have presented counterparts of these BICs in the circular array of rods. They compose a rather interesting feature, which is the partial filling of the inner space of the circular array. Note that one can consider the H-polarized near-BICs in the circular array of dielectric rods with similar results.

[1] S. Shipman and S. Venakides, Resonance and bound states in photonic crystal slabs, SIAM J. Appl. Math. **64**, 322 (2003).

[2] S. P. Shipman and S. Venakides, Resonant transmission near non robust periodic slab modes, Phys. Rev. E **71**, 026611 (2005).

[3] D. C. Marinica, A. G. Borisov, and S. V. Shabanov, Bound States in the Continuum in Photonics, Phys. Rev. Lett. **100**, 183902 (2008).

[4] R. F. Ndangali and S. V. Shabanov, Electromagnetic bound states in the radiation continuum for periodic double arrays of subwavelength dielectric cylinders, J. Math. Phys. **51**, 102901 (2010).

[5] C. W. Hsu, B. Zhen, J. Lee, S.-L. Chua, S. G. Johnson, J. D. Joannopoulos, and M. Soljačić, Observation of trapped light within the radiation continuum, Nature (London) **499**, 188 (2013).

[6] S. Weimann, Y. Xu, R. Keil, A. E. Miroshnichenko, A. Tunnermann, S. Nolte, A. A. Sukhorukov, A. Szameit, and Y. S. Kivshar, Compact Surface Fano States Embedded in the Continuum of Waveguide Arrays, Phys. Rev. Lett. **111**, 240403 (2013).

[7] C. W. Hsu, B. Zhen, S.-L. Chua, S. G. Johnson, J. D. Joannopoulos, and M. Soljačić, Bloch surface eigenstates within the radiation continuum, Light Sci. Applic. **2**, e84 (2013).

[8] B. Zhen, C. W. Hsu, L. Lu, A. D. Stone, and M. Soljačić, Topological Nature of Optical Bound States in the Continuum, Phys. Rev. Lett. **113**, 257401 (2014).

[9] Y. Yang, C. Peng, Y. Liang, Z. Li, and S. Noda, Analytical Perspective for Bound States in the Continuum in Photonic Crystal Slabs, Phys. Rev. Lett. **113**, 037401 (2014).

[10] E. N. Bulgakov and A. F. Sadreev, Bloch bound states in the radiation continuum in a periodic array of dielectric rods, Phys. Rev. A **90**, 053801 (2014).

[11] Z. Hu and Y. Y. Lu, Standing waves on two-dimensional periodic dielectric waveguides, J. Opt. **17**, 065601 (2015).

[12] J. M. Foley, S. M. Young, and J. D. Phillips, Symmetry-protected mode coupling near normal incidence for narrow-band transmission filtering in a dielectric grating, Phys. Rev. B **89**, 165111 (2014).

[13] M. Song, H. Yu, C. Wang, N. Yao, M. Pu, J. Luo, Z. Zhang, and X. Luo, Sharp Fano resonance induced by a single layer of nanorods with perturbed periodicity, Opt. Express **23**, 2895 (2015).

[14] C.-L. Zou, J.-M. Cui, F.-W. Sun, X. Xiong, X.-B. Zou, Z.-F. Han, and G.-C. Guo, Guiding light through optical bound states in the continuum for ultrahigh-Q microresonators, Laser Photon. Rev. **9**, 114 (2015).

[15] L. Yuan and Y. Y. Lu, Diffraction of plane waves by a periodic array of nonlinear circular cylinders, Phys. Rev. A **94**, 013852 (2016).

[16] Z. Wang, H. Zhang, L. Ni, W. Hu, and C. Peng, Analytical perspective of interfering resonances in high-index-contrast periodic photonic structures, IEEE J. Quantum Electron. **52**, 6100109 (2016).

[17] L. Yuan and Y. Y. Lu, Propagating Bloch modes above the lightline on a periodic array of cylinders, J. Phys. B **50**, 05LT01 (2017).

[18] Z. F. Sadrieva, I. S. Sinev, K. L. Koshelev, A. Samusev, I. V. Iorsh, O. Takayama, R. Malureanu, A. A. Bogdanov, and A. V. Lavrinenko, Transition from optical bound states in the continuum to leaky resonances: Role of substrate and roughness, ACS Photon. **4**, 723 (2017).

[19] I. Y. Polishchuk, A. A. Anastasiev, E. A. Tsyvkunova, M. I. Gozman, S. V. Solov'ov, and Y. I. Polishchuk, Guided modes in the plane array of optical waveguides, Phys. Rev. A **95**, 053847 (2017).

[20] E. N. Bulgakov and D. N. Maksimov, Light enhancement by quasi-bound states in the continuum in dielectric arrays, Opt. Express **25**, 14134 (2017).

[21] D. Colton and R. Kress, in *Inverse Acoustic and Electromagnetic Scattering Theory*, 2nd ed. (Springer, Berlin, 1998), p.165.

[22] M. G. Silveirinha, Trapping light in open plasmonic nanostructures, Phys. Rev. A **89**, 023813 (2014).

[23] E. N. Bulgakov and A. F. Sadreev, Bound states in the continuum with high orbital angular momentum in a dielectric rod with periodically modulated permittivity, Phys. Rev. A **96**, 013841 (2017).

[24] C. M. Linton and D. V. Evans, The interaction of waves with arrays of vertical circular cylinders, J. Fluid Mech. **215**, 549 (1990).

[25] H. D. Maniar and J. N. Newman, Wave diffraction by a long array of cylinders, J. Fluid Mech. **339**, 309 (1997).

[26] A. C. Ludwig, Wire grid modeling of surfaces, IEEE Trans. Antennas Propag. **35**, 1045 (1987).

[27] R. J. Paknys, The near field of a wire grid model, IEEE Trans. Antennas Propag. **39**, 994 (1991).

[28] D. V. Evans and R. Porter, Near-trapping of waves by circular arrays of vertical cylinders, Appl. Ocean Res. **19**, 83 (1997).

[29] G. Fikioris and K. Matos, Near fields of resonant circular arrays of cylindrical dipoles, IEEE Trans. Antennas Propag. **50**, 97 (2008).

[30] C. Sieutat, R. Peretti, J.-L. Leclercq, P. Viktorovitch, and X. Letartre, Strong confinement of light in low index materials: The photon cage, Opt. Express **21**, 20015 (2013).

[31] H.-b. Lü and X. Liu, Trapped modes with extremely high quality factor in the subwavelength ring resonator composed of dielectric nanorods, arXiv:1709.08006.

[32] D. Maystre, S. Enoch, and G. Tayeb, Scattering matrix method applied to photonic crystals, in *Electromagnetic Theory and Applications for Photonic Crystals*, edited by K. Yasumoto (Taylor & Francis, New York, 2006).

[33] L. N. Trefethen and J. A. C. Weideman, The exponentially convergent trapezoidal rule, SIAM Rev. **56**, 385 (2014).

[34] A. N. Oraevsky, Whispering-gallery waves, Quantum Electron. **32**, 377 (2002).

[35] *Handbook of Mathematical Functions*, edited by M. Abramowitz and I. Stegun (Dover Publication, New York, 1964).